ADVANCED MATERIALS

Supporting Information

for *Adv. Mater.*, DOI: 10.1002/adma.201500462

# Assembly of Colloidal Molecules, Polymers, and Crystals in Acoustic and Magnetic Fields

*Ye Yang, An T. Pham, Daniela Cruz, Christopher Reyes, Benjamin J. Wiley, Gabriel P. Lopez,* and Benjamin B. Yellen**

Supporting Information

**Assembly of Colloidal Molecules, Polymers, and Crystals in Acoustic and Magnetic Fields**

Ye Yang[1,5], An T. Pham[1,5], Daniela Cruz[2,5], Christopher Reyes[3,5], Benjamin Wiley[3,5], Gabriel P. Lopez[1, 2, 5], and Benjamin B. Yellen[1, 2, 4, 5]

[1]Duke University, Department of Mechanical Engineering and Materials Science, Box 90300 Hudson Hall, Durham, NC, USA 27708
[2]Duke University, Department of Biomedical Engineering, Durham, NC, USA 27708
[3]Duke University, Department of Chemistry, Durham, NC, USA 27708
[4]University of Michigan - Shanghai Jiao Tong University, Joint Institute, Shanghai Jiao Tong University, 800 Dong Chuan Rd, Shanghai, China, 200240
[5]NSF Research Triangle Materials Research Science and Engineering Center (MRSEC)

## 1. Analytical Calculation:

The potential energy of interacting, spherical paramagnetic particles in an external magnetic field is modeled as an ensemble of point dipoles at the centers of hard spheres. The system potential energy $U$ has three contributions, including: (1) magnetic interactions between induced point dipoles, (2) gravitational energy associated with out-of-plane particle displacements, and (3) surface adhesion energy between two spheres, summed as:

$$U = \sum_{i<j}^{N} U_{\mathrm{dd}}\left(\boldsymbol{r}_{ij}\right) + U_{\mathrm{g}}\left(\boldsymbol{r}_{i}\right) + U_{\mathrm{s}}\left(\boldsymbol{r}_{ij}\right) \tag{1}$$

where $r_{ij}$ is the distance between particles $i$ and $j$. The dipolar interaction energy is expressed as:

$$U_{dd}(\mathbf{r}_{ij}) = -\frac{\mu_0}{4\pi r_{ij}^3}\left[3\left(\boldsymbol{m}_i \cdot \hat{\boldsymbol{r}}_{ij}\right)\left(\boldsymbol{m}_j \cdot \hat{\boldsymbol{r}}_{ij}\right) - \boldsymbol{m}_i \cdot \boldsymbol{m}_j\right], \tag{2}$$

where $\boldsymbol{m_i}$ and $\boldsymbol{m_j}$ are the effective dipole moments and $\hat{\mathrm{x}}$ is a unit vector.

The effective magnetic susceptibility of a spherical particle submersed in water is given by:

$$\bar{\chi} = 3\left(\frac{\mu_p - \mu_0}{\mu_p + 2\mu_0}\right), \tag{3}$$

where particles are assumed to have homogeneous magnetic permeability, $\mu_p$. The effective dipole moment of the particles is thus:

$$\boldsymbol{m} = \bar{\chi} v \boldsymbol{H}, \tag{4}$$

where $v$ is the particle volume, and the total field $\boldsymbol{H}$ contains results from the external field and the field created by other inducible dipoles. We assumed that structures not in direct contact with other particles were sufficiently well separated su that their field contributions were ignored in the self-consistent calculations. The magnetic moments are solved self-consistently only for the interactions between directly touching particles by simultaneous solution of the system of equations:

$$\boldsymbol{m}_i = \bar{\chi}_i v_i \left[ \boldsymbol{H} + \sum_{j \in \partial i(\boldsymbol{m})} \frac{3(\boldsymbol{m}_j \cdot \hat{r}_{ij})\hat{r}_{ij} - \boldsymbol{m}_j}{4\pi r_{ij}^3} \right] \tag{5}$$

where the total field includes the external field, $\boldsymbol{H}$, as well as the field due to the $j$ particles in direct (or nearly direct) contact with particle $i$. As an example, for the dimer, trimer, and tetramer phases, the individual structures have 2, 3, and 4 particles, respectively, which are included in the self-consistent moment calculations. For the chain phase, there are $j = 2$ nearest neighbors for each particle, which is the periodic unit cell in the infinite chain and is similar to the central particle in a trimer structure.

Due to the small magnetic fields, and thus low magnetic potential energies, gravity was found to be an important contributor to the overall particle energies. The magnetic particles are heavier than the carrier fluid with density mismatch $\rho = 400\text{kg/m}^3$, and thus the gravitational contribution was:

$$U_g(\boldsymbol{r}_{ij}) \equiv \bar{\rho} v g \boldsymbol{r} \cdot \hat{z} \tag{6}$$

where $v$ is the volume of a bead of type $i$ and the $z = 0$ plane is at a distance $\sigma/2$, above the bottom glass slide. In the dimer, trimer, and tetramer structures, there is only one particle in contact with the top slide, while the other particles are resting on the bottom slide. For the chain phase, one half of the particles are in contact with each glass slide.

The surface adhesion energy of two spherical particles was modeled as a Van der Waals (VW) type attraction between two polystyrene spheres across water,

$$U_s(\boldsymbol{r}_{ij}) = -A\sigma/24D, \tag{7}$$

with the Hamaker constant for polystyrene/water/polystyrene interface taken to be the typical value of $A$=1.3×10$^{-20}$ J.[1] The variables $\sigma$ and $D$ represent the particle diameter, and the separation distance between the opposing surfaces, respectively. By fitting the experimental data to the theoretical model, we determined that the energy gain two particles achieved by coming into direct contact was approximately 6.5×10$^{-20}$ J, which is similar to the surface adhesion energies used in modeling other colloidal systems, corresponding to about 10-15 $k_BT$. This value corresponds to the VW attraction for two particles separated by $D$=25 nm, which is similar to the Debye length of particle in an aqueous solution with 0.1 mM monovalent ion concentration, e.g., a solution with pH ~4. Due to the strong distance dependence on the separation distance, this energy gain was only included for particles in direct contact. For the dimer, trimer, and tetramer structures, respectively, there were 1, 2, and 3 surface adhesion bonds used in the potential energy calculations. For the chain structures, we assumed one bond per particle.

The average (per particle) potential energies of the monomer, dimer, trimer, tetramer, and chain structures were calculated as function of the volume fraction of particles, $\eta$. In order to simulate an infinite system, the interaction energy between the central structure and the rest of structures was calculated inside a square slab with side length of 100σ and thickness of $h$ = 1.42$\sigma$. The particles in contact with the top slide thus had their centers located at a height of $z$ = 0.92$\sigma$. For the purpose of efficient summation, each discrete colloidal structure is assumed to have identical orientation and is arranged in a hexagonal lattice to maximize inter-structure separation distance. The coordinates for the monomer, dimer, trimer, and tetramer structures were generated by arranging a hexagonally packed monolayer, with the base particle resting on the bottom glass slide (Figure S1). The equilibrium separation distance, $d$, between structures can be expressed as:

$$d=\sigma(n\pi/3\sqrt{3}h\eta)^{1/2}, \quad (8)$$

where $\eta$ is the volume fraction of particles, and $n$=1, 2, 3, 4 is the number of particles in the cluster. The chain structures were assumed to be arranged in a parallel linear array with the interchain separation distance defined as:

$$d=\pi\sigma^2/6h\eta sin(\psi/2), \quad (9)$$

where the bond angle between nearest particles in the chain is assumed to be $\psi$=130$^o$.

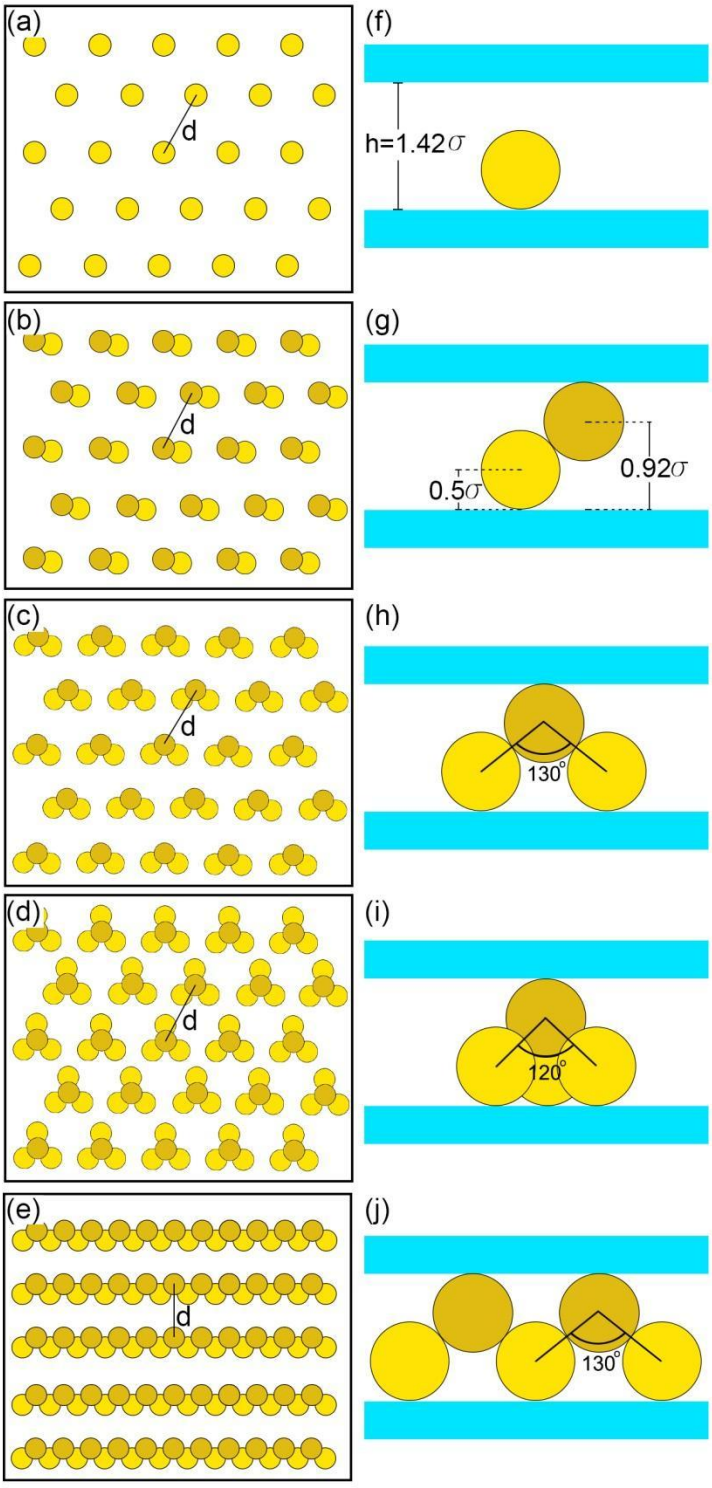


**Figure S1. Structural configurations used in the potential energy comparison**. The top-down and side view of monomers are demonstrated in (a) and (f). Similarly, top/side views of dimers, trimers, tetramers and chains are illustrated in (b)/(g), (c)/(h), (d)/(i) and (e)/(j) respectively. The fluid film heights and bond angles are also noted.

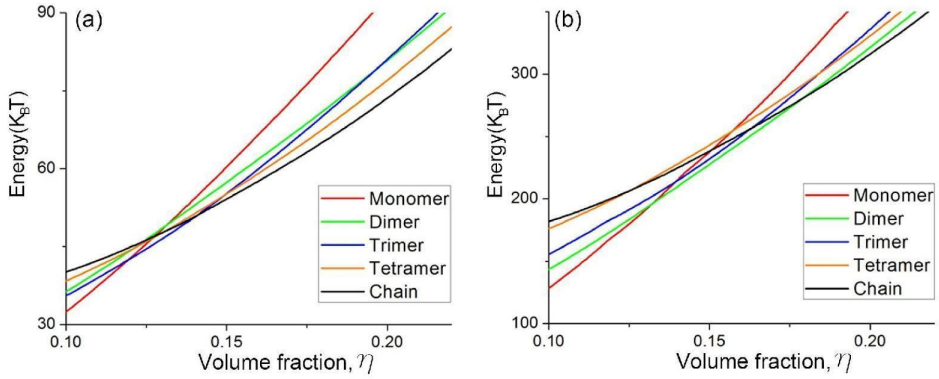


**Figure S2. Potential energy comparison of the different phases.** Energy plots for hexagonally packed arrays of monomers, dimers, trimers, tetramers, and linearly spaced chain structures are demonstrated for (a) H=6Oe and (b) H=12Oe in the concentration range of $0.10 < \eta < 0.25$. Dimer phases are never the lowest energy phase at H=6Oe, but they become the minimum energy configuration for $0.12 < \eta < 0.18$.

The average (per particle) potential energy of the monomer, dimer, trimer, tetramer, and chain structures were calculated as function of the volume fraction for weak (H=6Oe, corresponding to T*=0.068) and strong field (H=12Oe, corresponding to T*=0.017), and the resulting energy curves are presented in Figure S2. The potential energy plot at H=6Oe (T*=0.068) (Figure S2a and Figure 2h) is approximately consistent with our experimental results (Figure 2g). In this case, the dimer phase is rarely observed in experiments, and likewise does not represent the minimum energy phase for any volume fraction. The absence of dimers can be attributed to the increased importance of the gravity terms and surface adhesion energies at low field strengths. At higher field strengths of H=12 Oe (T*=0.017), dimers become the minimum energy configuration for $0.12 < \eta < 0.18$, due to the increased importance of the magnetic interactions. These results thus imply that individual clusters (dimer, trimers, etc.) can be selected by carefully controlling the magnitude of the interparticle interactions.

This trend is also confirmed experimentally, in which we assembled particles at a constant volume fraction of $\eta \sim 0.13$, but at different external field strengths ranging from 1.5 - 12 Oe. Below 3.5 Oe ($T^*>0.200$), gravity dominated the interactions and only monomers were observed. Between 3.5 Oe ($T^*=0.200$) and 5.5 Oe ($T^*=0.081$), trimers

were the predominantly observed cluster, whereas dimers were absent. Above 5.5 Oe ($T^*$=0.081), the ratio of trimers to dimers gradually decreased to zero at fields above 12 Oe ($T^*$=0.017). (Figure S3). Details of the corresponding relationship between field strength and pairwise interaction between two particles in contact can be found in Table 2. (Page 15 of Supplementary Information).

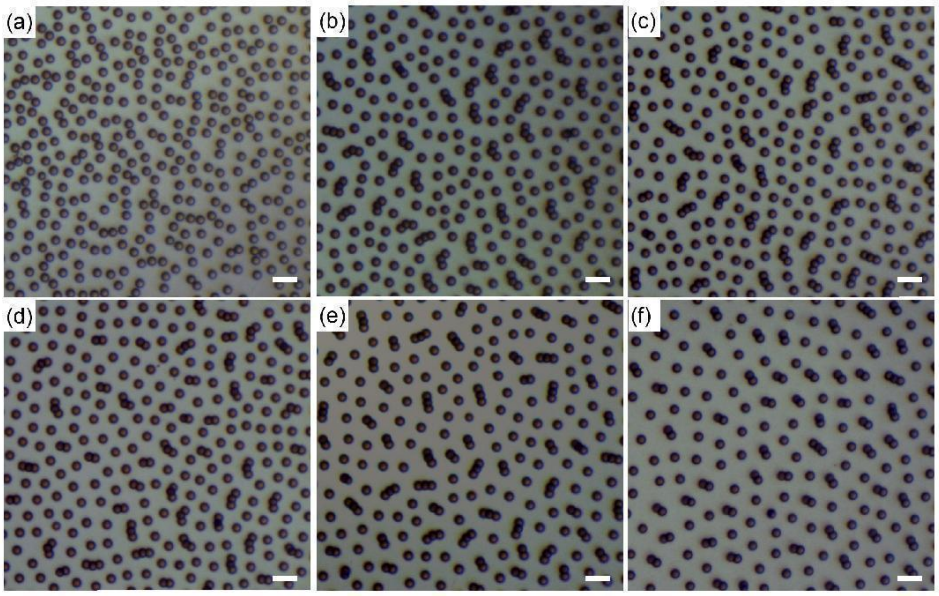


**Figure S3. Dimers and trimers formed at different vertical fields.** For $\eta \sim 0.13$, the assembled structures are depicted as a function of increasing field strength: (a) H=1.5Oe, (b) H=3.5Oe, (c) H=5.5Oe, (d) H=8Oe, (e) H=10Oe and (f) H=12Oe. The scale bars in the all images are 10μm.

## 2. Molecular Dynamics (MD) Simulation

The molecular dynamics simulation was implemented with LAMMPS[2] using Langevin Dynamics. For a colloidal particle i, the equation can be expressed as:

$$m\boldsymbol{a}_i = \boldsymbol{F}_c + \boldsymbol{F}_f + \boldsymbol{F}_r \tag{10}$$

where $m$ is mass of the particles, $\boldsymbol{F_f}$ is the viscous resistance experienced by the relative movement of colloid in uniform fluid. The resistance force is given by: $\boldsymbol{F_f}=-m\mathrm{v}/\tau$, where v is the velocity of the particle and $\tau=m/(3\pi\gamma\sigma)$ is the Stoke's damping parameter on a spherical particle in a solvent with viscosity, $\gamma$. The random force of thermal fluctuation is denoted by $\boldsymbol{F_r}$, while $\boldsymbol{F_c}$ is the force induced by the particle particle interactions:

$$\boldsymbol{F}_c = -\nabla U_i \tag{11}$$

In the MD simulations, we modeled the particle interactions as a sum of magnetic

dipole-dipole interactions, hard sphere interactions, and gravitational energy. The hard sphere interactions were approximated with Lennard-Jones potential with a cut-off distance, expressed as:

$$U_{LJ}(r_{ij}) \approx \begin{cases} 4\varepsilon\left[\left(\dfrac{\sigma}{r_{ij}}\right)^{12} - \left(\dfrac{\sigma}{r_{ij}}\right)^{6}\right] & r_{ij} < r_c \\ 0 & r_{ij} \geq r_c \end{cases} \quad (12)$$

Where $\varepsilon$ is the depth of the potential well which was set as surface adhesion energy of two spherical particles calculated from Eq (7), $\sigma$ is the particle diameter, and $r_c$ is the cut-off distance, which was set to be $r_c = \sigma$. When we increased the cut-off radius to include short range attractions in the Lennard-Jones potential, there was only minor improvement in the agreement between theory and experiment for this particular simulation package. Thus, we chose a hard sphere cutoff in the MD simulations.

Simulations employed a box with dimensions $L_x$=15$\sigma$, $L_y$= 15$\sigma$, $L_z$= 1.5$\sigma$, in which periodic boundary condition were applied in the planar directions, whereas a reflecting boundary condition was used in the vertical direction to simulate the spatial confinement. We used the velocity Vervet algorithm[3] for time integration, where the characteristic time $\tau_c=\sigma(m/\varepsilon)^{1/2}$ was approximately $9\times10^{-4}$ s, and the simulations used $\Delta t$=0.001$\times\tau_c$ as time steps. The dimensionless parameters were chosen based on well-established methods[3] and defined in Table 1. The reduced temperature was set to $T^*=k_BT/\varepsilon$ , where $k_B$ and $T$ are the Boltzmann constant and temperature, respectively. The dimensionless time, was $\Delta t^*=(\varepsilon/m\sigma^2)^{1/2}$. The reduced dipole moment was calculated as $\boldsymbol{m}^* = \boldsymbol{m}/(4\pi\sigma^3\varepsilon/\mu_0)^{1/2}$ with $\mu_0$ is permeability of free space.

| Parameter | Real Units | Reduced Units | Description |
|---|---|---|---|
| $\sigma$ | 3 μm | $\sigma^*=\sigma/\sigma$=1 | Diameter |
| $L_z$ | 45 μm | $L_x^*=L_z/\sigma$=15 | Width of simulation box |
| $L_y$ | 45 μm | $L_y^*=L_z/\sigma$=15 | Length of simulation box |
| $L_z$ | 4.5 μm | $L_z^*=L_z/\sigma$=1.5 | Height of simulation box |
| $r_c$ | 3 μm | $r^*_c=r_c/\sigma$=1 | Cut-off distance |
| $\varepsilon$ | $6.5\times10^{-20}$ J | $\varepsilon^*=\varepsilon/\varepsilon$=1 | Depth of potential well |
| $m$ | $5.652\times10^{-15}$ kg | $m^*=m/m$=1 | Mass |
| $g$ | 9.81 m/s$^2$ | $g^*=gm\sigma/\varepsilon$=2.56 | Gravitational accelaration |
| $\Delta t$ | $9\times10^{-7}$ s | $\Delta t^*=\Delta t(\varepsilon/m\sigma^2)^{1/2}$ =0.001 | Time step |
| $\boldsymbol{m}$ | $5.433\times10^{-15}$ A.m$^2$ | $\boldsymbol{m}^*=\boldsymbol{m}/(4\pi\sigma^3\varepsilon/\mu_0)^{1/2}$=1.3 | Dipole moment |
| $T$ | 300 K | $T^*=k_BT/\varepsilon$=0.064 | Temperature |

| | | | |
|---|---|---|---|
| $\tau$ | $2.24\times10^{-8}$ s | $\tau^*=\tau(\varepsilon/m\sigma^2)^{1/2}/\Delta t^*=0.025$ | Damping time |
| $\tau_c$ | $9\times10^{-4}$ s | | Characteristic time |
| $\gamma$ | $8.9\times10^{-5}$ N s/m$^2$ | | Viscosity |
| $\rho$ | 400 kg/m$^3$ | | Density |
| $\|H\|$ | 6 Oe | | Magnetic field |
| $\mu_0$ | $4\pi\times10^{-7}$ H/m | | Permeability of vacuum |
| $\mu_p$ | $2.1\mu_0$ | | Permeability of particles |
| $D$ | 25 nm | | Separation distance |
| $A$ | $1.3\times10^{-20}$ J | | Hamaker constant |
| $k_B$ | $1.38064\times10^{-23}$ J/K | | Boltzmann constant |
| $\chi$ | 0.8 | | Susceptibility |
| $h$ | $1.42\sigma$ | | Film thickness |
| $\psi$ | $130^o$ | | Bond angle |
| $v$ | $1.414\times10^{-17}$ m$^3$ | | Volume of particle |
| $\eta$ | | | Volume fraction |
| v | | | Velocity of particle |

Table 1: Parameters used in analytical calculation and MD simulations

Based on an assumed volume fraction, we adjusted the number of particles in the simulation box. The particle number was maintained above an arbitrary threshold allowing for consistently low numerical error. For each volume fraction concentration, the MD simulation was performed for at least $10^5$ time steps without magnetic field in order to provide time to randomize the particle distribution and achieve thermal equilibrium, which was verified by monitoring the system energy. Next, we ran the MD algorithm for at least $10^5$ time steps in the presence of an external magnetic field, again verifying equilibriation by monitoring the system energy.

The results at different concentration and field strengths were demonstrated in Figure S4, which for the most part is qualitatively consistent with both analytical calculation and experiments. However, we note that there are a few qualitative differences between the MD simulations and experiments. For example, in experiments we find that the tetramer structures are relatively stable for $0.14 < \eta < 0.17$ at H = 6Oe ($T^*=0.068$), while they are observed to be stable only at H=18Oe ($T^*=0.0075$) in MD simulations. We also find that the cross-linked chain networks were observed at $0.3 < \eta < 0.4$, which were rarely observed in the experiment (Figure 1c). We also found that the non-closed-packed hexagonal lattices, which were frequently observed in experiments (Fig. 2e), were never observed in MD simulations at $\eta < 0.4$ regardless of the field

strength. They were not observed even when we increased the cutoff radius to add a soft sphere attractive interaction, which indicates that perhaps not all the interactions are being completely accounted for in our model. On the other hand, the non-close-packed square lattices (or square network) were rarely observed in experiments (Figure 1c), however it was frequently observed at $\eta \sim 0.3$ in MD simulation (Figure S4, p and q).

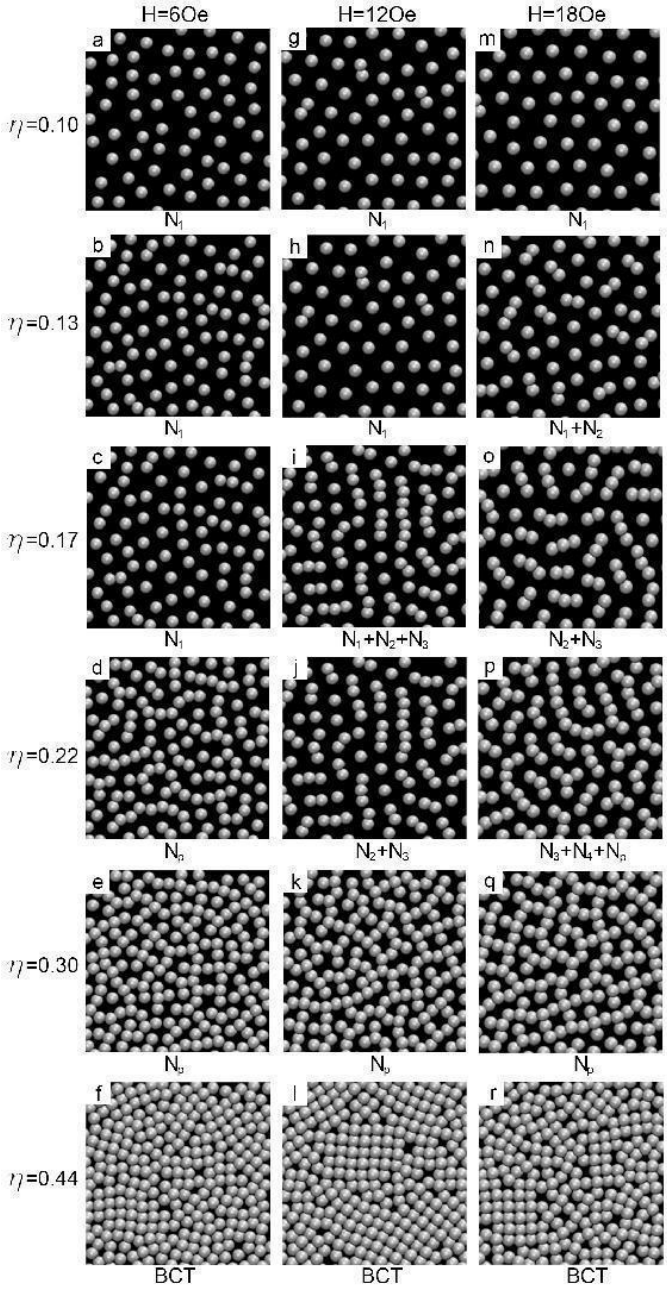


**Figure S4. Molecular Dynamics simulations of particles assemblies in different field strengths and**

**volume fractions.** The columns correspond to MD simulations at different field strengths, while the rows correspond to simulations at different particle concentrations. The dominant structures at each condition are denoted beneath the image: monomers, dimers, trimers and tetramers are named as $N_1$, $N_2$, $N_3$, $N_4$, respectively, while chains are named as $N_p$ (standing for polymers), and body-centered-tetragonal are named as BCT.

We were unable to adjust the vertical confinement of the fluid film with sub-micron precision. Instead, we performed MD simulations over different fluid thicknesses in order to gain insight into the effect of vertical confinement. The results at different particle concentrations and chamber thicknesses are presented in Figure S5. In strongly confined systems (fluid thickness, $h \leq 1.3\sigma$), we observed that the formation of colloidal molecules, and polymers was strongly suppressed (Figure S5, Column 1), due to the inability of the particles to buckle in the vertical dimension. In strong confinement, the particle interactions are predominantly repulsive and leads to non-close-packed arrays of monomers at low and medium particle concentration (Figure S5, a-d), and approaching hexagonally close-packed (HCP) lattices at high particle concentration (Figure S5, f). In weakly confined systems (fluid thicknesses of $1.3\sigma \leq h \leq 1.7\sigma$), we observed a variety of new structures, including colloidal molecules (Figure S5j), polymers (Figure S5k) and body-centered-tetragonal (BCT) lattices (Figure S5l). These new structures are observed due to the ability for particles to buckle in the vertical direction, which reduces the magnetic repulsion. The delicate balance between surface attraction, reduced magnetic repulsion, and gravitational interactions leads a variety of new structures that are not observed in strongly confined systems. We note in MD simulations that adjusting the degree of confinement from $1.3\sigma$ to $1.7\sigma$ did not lead to a fundamentally different class of structures, though it did allow for variation in the bond angles of the colloidal molecules, polymers, and crystals, and can change the concentration range over which they appear.

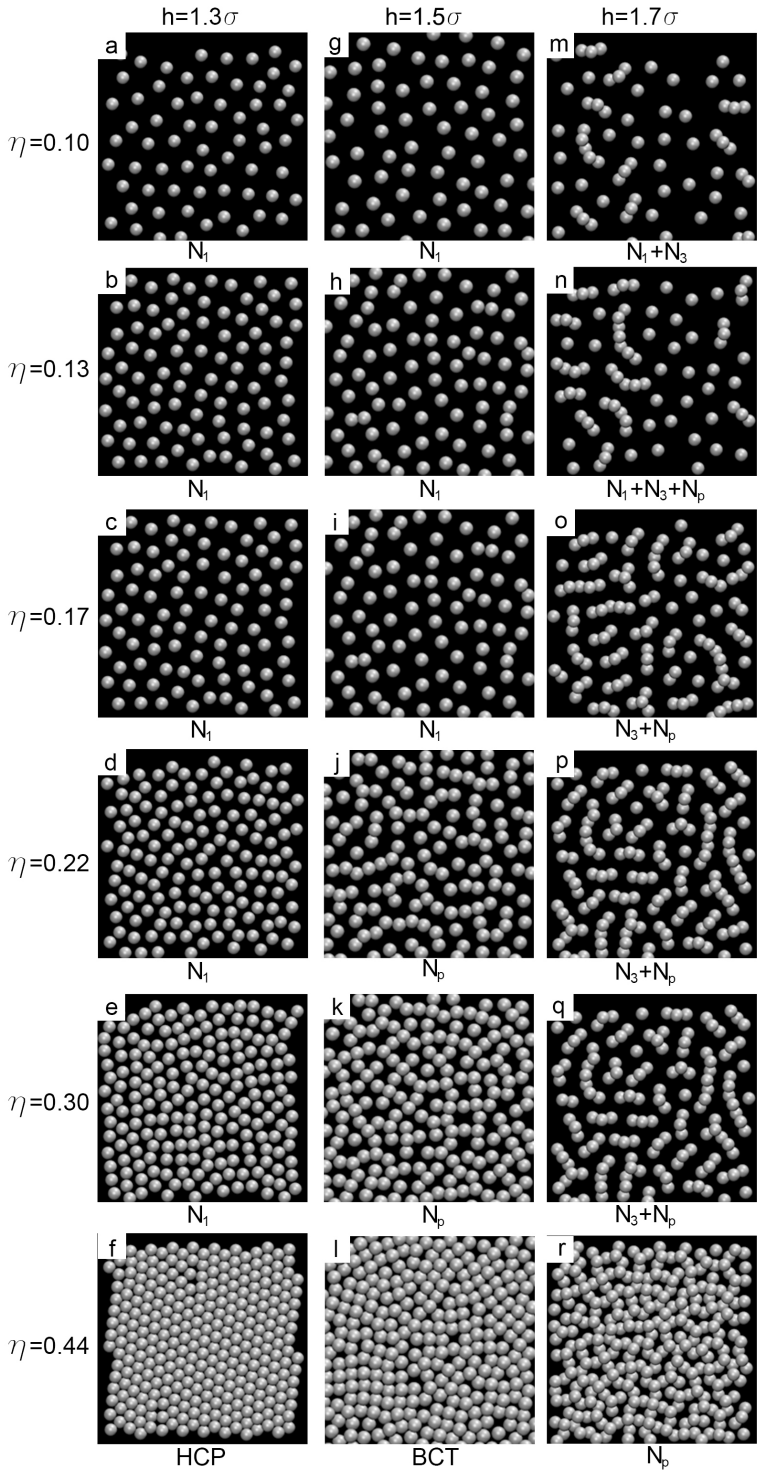


**Figure S5. Molecular Dynamics simulations of particles assemblies with different confinement (chamber thickness).** The columns correspond to MD simulations at different chamber, while the rows correspond to simulations at different particle concentrations. The dominant structures at each condition are denoted beneath the image: monomers, dimers, trimers and tetramers are named as $N_1$, $N_2$, $N_3$, $N_4$, respectively, while chains are named as $N_p$ (standing for polymers), and body-centered-tetragonal are named as BCT.

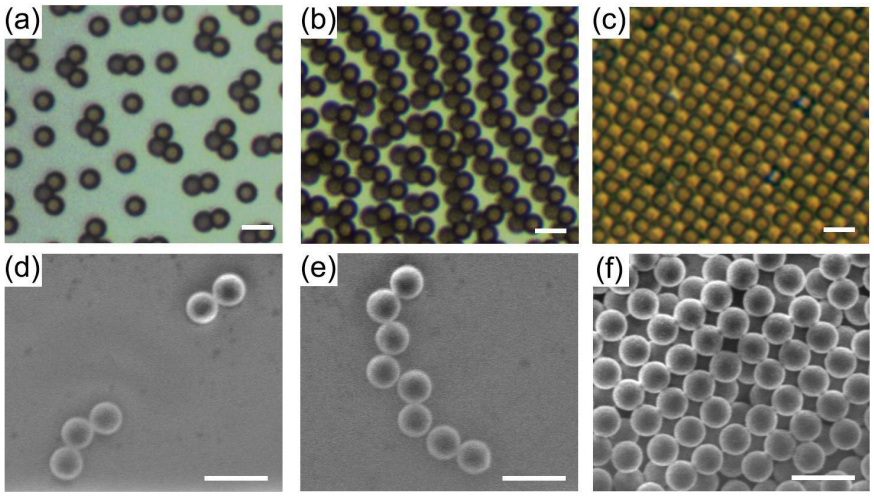


**Figure S6. Stabilization and drying of colloidal structures.** The colloidal structures can be stabilized with the addition of photoacids, and some of the structures can be dried for SEM images. The optical images in the magnetoacoustic assembly process are shown for (a) dimers/trimers, (b) zigzag chains and (c) BCT lattice. Corresponding SEM images of the dried structures after stabilization are shown for (d) dimers/trimers, (e) zigzag chains, and (f) BCT lattice. The scale bars in the all images are 5μm.

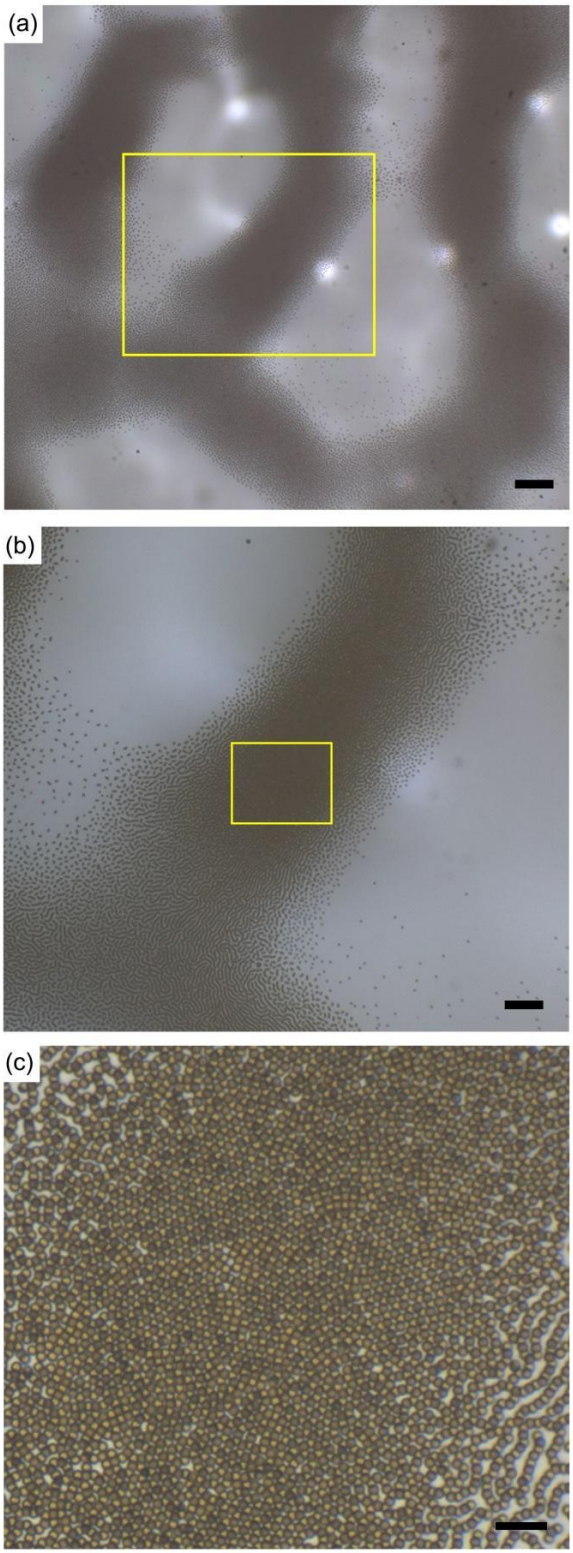


**Figure S7. Demonstration of multi-scale assemblies.** The colloidal assemblies with meso scale arrangements are demonstrated under (a) 5x objective and (b) 10x objective. The corresponding micro-scale structures are demonstrated under (c) 40x objective. Yellow rectangles in (a) (and (b)) indicate the region of interest in the zoomed image (b) (and (c)).

| Field Strength (Oe) | $T^*$ |
|---|---|
| 1.5 | 1.087 |
| 3.5 | 0.200 |
| 6 | 0.0682 |
| 8 | 0.0383 |
| 10 | 0.0245 |
| 12 | 0.0170 |
| 18 | 0.0076 |

Table 2. Correlation of Field Strength with Effective tempearature.

**Movie caption:**

**Movie M1. Phase transformation induced by pressure change**

The phase transformation from non-close-packed hexagonal (n-HCP) lattice into body centered tetragonal (BCT) lattice induced by increase of acoustic field is demonstrated. The magnetic field was kept constant at 6Oe, while the input signal of the acoustic field was instantly increased from 5V to 10V at the beginning of the movie. The movie was 166 times faster than real time, which corresponds to an experimental time of 2000 seconds.

**Movie M2. Demonstration of structure stabilization with photoacids**

Chain structures were formed by applying an in-plane magnetic field to a suspension of paramagnetic colloidal particles dispersed in 0.1M photoacid solution (pyranine). The field strength was held constant at H=20Oe for 4 hour during exposure to 36 mw/cm$^2$ radiation at 365 wavelength. After UV exposure, the magnetic field was removed, and the movie demonstrates that the chain structures remain stable during mechanical perturbation of the fluid chamber. The movie is presented in real time.

**Reference**

[1] J. N. Israelachvili, *Intermolecular and surface forces* **2011**, Academic Press.

[2] S. J. Plimpton, *J. Comput. Phys.* **1995**, 117, 1.

[3] M. P. Allen, D. J. Tildesley, *Computer simulation of liquids* **1989**,Oxford University Press.